Computers and Concrete, *Vol. 24, No. 4 (2019) 283-293*
DOI: https://doi.org/10.12989/cac.2019.24.4.283

Experimental and numerical simulation study on fracture properties of self-compacting rubberized concrete slabs

Jiajia Wang[1,2], Xudong Chen[*2], Jingwu Bu[1,3] and Shengshan Guo[4]

[1]State Key Laboratory of Hydrology-Water Resources and Hydraulic Engineering, Hohai University, Nanjing, 210098, P.R. China
[2]College of Civil and Transportation Engineering, Hohai University, Nanjing, 210098, P.R. China
[3]College of Hydraulic and Energy Power Engineering, Yangzhou University, Yangzhou, 225009, P.R. China
[4]China Institute of Water Resources and Hydropower Research, Beijing, 100048, P.R. China

(*Received February 26, 2019, Revised July 23, 2019, Accepted August 6, 2019*)

Abstract. The limited availability of raw materials and increasing service demands for pavements pose a unique challenge in terms of pavement design and concrete material selection. The self-compacting rubberized concrete (SCRC) can be used in pavement design. The SCRC pavement slab has advantages of excellent toughness, anti-fatigue and convenient construction. On the premise of satisfying the strength, the SCRC can increase the ductility of pavement slab. The aim of this investigation is proposing a new method to predict the crack growth and flexural capacity of large-scale SCRC slabs. The mechanical properties of SCRC are obtained from experiments on small-scale SCRC specimens. With the increasing of the specimen depth, the bearing capacity of SCRC beams decreases at the same initial crack-depth ratio. By constructing extended finite element method (XFEM) models, crack growth and flexural capacity of large-scale SCRC slabs with different fracture types and force conditions can be predicted. Considering the diversity of fracture types and force conditions of the concrete pavement slab, the corresponding test was used to verify the reliability of the prediction model. The crack growth and flexural capacity of SCRC slabs can be obtained from XFEM models. It is convenient to conduct the experiment and can save cost.

Keywords: self-compacting rubberized concrete (SCRC); crack growth; flexural capacity; extended finite element method (XFEM)

1. Introduction

With the development of the automobile and rubber industry, the number of waste tires is soaring. The recycling of waste tires has become a severe environmental problem (Tao 2017). Recycling of waste tires can improve the environment, such as the application of rubber concrete. At present, cracks of ordinary concrete pavement are universal. Compared with ordinary concrete, rubber concrete can increase the toughness and anti-fatigue performance of pavement and reduce noise pollution (Zhu *et al*. 2018, Khaloo *et al*. 2008, Taha *et al*. 2008, Turgut and Yesilata 2008, Sukontasukkul and Chaikaew 2006). With good fluidity, Self-compacting concrete (SCC) has advantages of convenient construction and low labor cost, and can be widely used in road engineering. Compared with ordinary concrete, SCC is resource-saving and environmentally friendly. (Long *et al*. 2015, Venkateswara *et al*. 2012, Gencel *et al*. 2015). At present, some scholars mainly investigate SCRC basic mechanical properties and durability (Najim 2012, Yung *et al*. 2013). However, the fracture problem of SCRC is ignored. Fracture mechanics is a useful tool to investigate crack growth and flexural capacity. So the knowledge of fracture mechanics is used to investigate the SCRC.

∗Corresponding author, Professor
E-mail: xdchen@hhu.edu.cn

Many scholars have carried out a lot of experimental research on fracture properties of ordinary concrete pavement (Bu *et al*. 2018, Zak *et al*. 2006, Hou *et al*. 2014, Dong *et al*. 2018). Sub-standard raw materials and non-conformity of construction techniques are primary reasons for the fracture of ordinary concrete pavement. If the raw materials are sub-standard, it will seriously influence the quality of the concrete, and there will be more diseases in the early stage. If the construction techniques are non-conformity, it will lead to the concrete is not dense and uniform. Long vibrating time make concrete form segregation, the coarse aggregate will sink into the bottom, the fine aggregate will stay in the upper layer, the strength distribution will be uneven, and the surface shrinkage crack will increase (Gao 2007, Wang 2012). The SCRC has vast superiority in road engineering. The application of the SCRC can improve the performance of the pavement, but the investigation on the fracture property of SCRC pavement slab is not perfect yet (Hesami *et al*. 2016), so it is significant to investigate the fracture properties of the SCRC pavement (Modarres and Shabani 2015, Fakhri and Amoosoltani 2017).

The Mechanistic-Empirical Pavement Design Guide (MEPDG) (Kim and Lee 2002, Merhej and Feng 2011) is used to design the thickness of rigid pavement based on the estimated load, foundation soil condition, and hardened concrete property. The MEPDG is a new method for pavement design and analysis. The guide considers parameters that influence pavement performance, including

http://www.techno-press.org/?journal=cac&subpage=8
ISSN: 1598-8198 (Print), 1598-818X (Online)

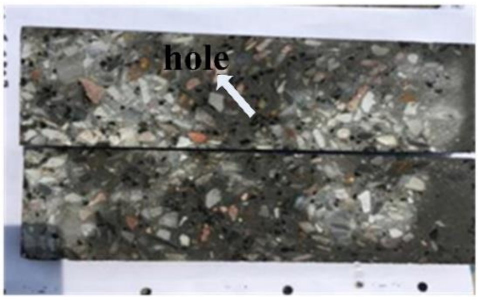

Fig. 1 Non-Uniform distribution of rubber particles

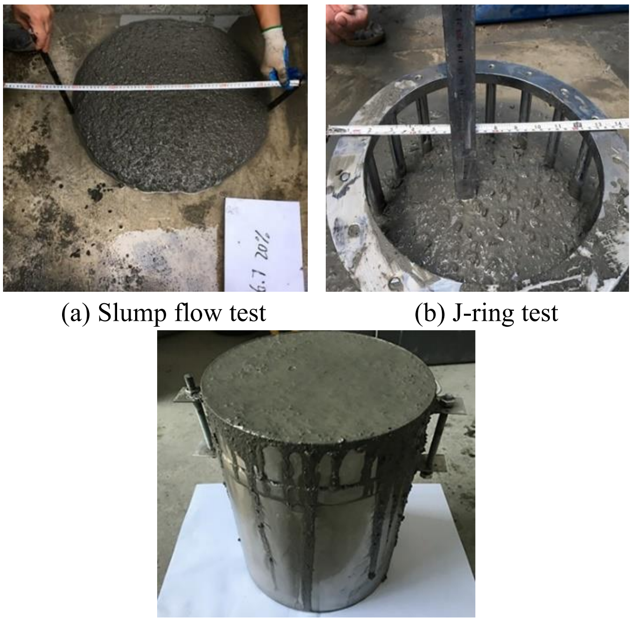

(a) Slump flow test (b) J-ring test

(c) Segregation test

Fig. 2 Test on fresh SCC

Fig. 3 Uniform distribution of rubber particles

traffic, climate, pavement structure and material properties, and applies the principles of engineering mechanics to predict critical pavement responses. Protective measures for concrete pavement lack theoretical knowledge and need further research.

Many scholars use the extended finite element method (XFEM) to investigate the fracture properties of concrete (Skarżyński *et al*. 2015, Kumar *et al*. 2014). The XFEM is based on the traditional finite element added functions, and it can reflect the discontinuity of the jump function and the rowing displacement field of the crack tip. In the XFEM, the mesh and crack are independent of each other, so the local mesh encryption method is unnecessary for crack propagation. During calculating, the crack growth of arbitrary path can be described, and it is convenient to apply heterogeneous material (Gaedicke *et al*. 2012, Zi and Belytschko 2010, Singh *et al*. 2012, Zhai *et al*. 2017). Using the XFEM to investigate the fracture process of the pavement slab is effective.

This paper investigates a new method to predict the crack growth and flexural capacity of large-scale SCRC slabs. By constructing the XFEM model, crack growth and flexural capacity of large-scale SCRC slabs with different fracture types and force conditions can be predicted. The material properties of large-scale SCRC slabs are obtained from a beam on the TPB test. The properties of foundation soil are obtained from beams on a soil test. Considering the diversity of fracture types and force conditions of the concrete pavement slabs, the corresponding tests are used to verify the reliability of the prediction model.

2. Experimental program

2.1 Specimen preparation

The mix composition of the concrete is determined according to the content of the fixed volume the aggregate method. Since the maximum replacement of rubber particles has been recommended to be below 30% (Zheng *et al*. 2008), considering that the addition of rubber particles will reduce the strength of concrete, rubber content of 10% of the total fine aggregate volume was adopted. One of the common problems of rubber concrete is the uneven distribution of rubber particles, dense rubber particles will form a “hole”, as shown in Fig. 1. The uneven distribution of rubber particles makes the strength of rubber concrete decrease sharply, which affects the fracture properties of rubber concrete. A large number of other admixtures were tested to find a method to ensure rubber particles can distribute evenly in the mixture, and finally found that the addition of polycarboxylic water reducer can make distribution of rubber particles more uniform. The problem of uneven distribution of rubber particles is solved, the strength and fracture mechanical properties of rubber concrete are improved. Fly ash and silica fume can improve the compactness, the long-term strength and durability of self-compacting concrete. The optimum content of fly ash and silica fume was determined by tests. To evaluate the workability of the fresh SCRC, the slump flow test, J-ring test and segregation test were performed, as shown in Fig. 2. The results of tests are displayed in Table 1. The results demonstrate that the SCRC meets the requirement of self-compacting concrete. The determined mix proportion is shown in Table 2.

The raw materials used in the test include CEM I 42.5R Portland cement, crushed stone whit with the particle size below 20 mm, sand with the density of 2600 kg/m^3, fly ash, silica fume and rubber whose density is 1060 kg/m^3 and content accounts for 10% of the total fine aggregate volume. The rubber is obtained by shredding the worn-out scrap car tires and was sieved to get rubber particles with a maximum size of 0.5 mm. The water-binder ratio is 0.364

Table 1 Workability of fresh concrete

	SCRC-10
Slump flow (mm)	695
J ring flow (mm)	661
Difference between slump flow and J ring flow (mm)	34
Δh (mm)	6
Segregation (%)	5.4

Table 2 The mixture proportion of materials used in the experiments

Material consumption (kg/m^3)							Plasticizer (kg/m^3)
Cement	Water	Fly ash	Silica fume	Gravel	Rubber	Sand	
385	200	139	26	800	41.5	916.2	7.5

Table 3 Condition of the SCRC beam

Experiment type	α	Specimen size (length, depth, width) (mm^3)	Number	Loading rate (mm/s)
Beam loading (On TPB test)	0.3	1200×250×100	3	0.001
	0.3	800×150×100	3	0.001
	0.3	400×100×100	3	0.001
Beam loading (On soil test)	0.3	1200×250×100	3	0.001
	0.3	800×150×100	3	0.001
	0.3	400×100×100	3	0.001

and the sand content is 52% of the total aggregate mass in the test. Crushed stone and sand are employed as the coarse and fine aggregate.

The reason why the distribution of rubber particles is uneven was obtained through making different formulation test. The main reasons are as follows: (1) The coagulation time of concrete is short, and the fluidity of concrete is poor. The rubber particles gather into a "hole" easily; (2) Rubber particles introduce many bubbles, and its density is low. To reduce the formation of bubbles and increase the fluidity of concrete, the defoamer and retarder were added into the concrete. After attempts, the rubber particles are still uneven. Through a large number of other admixtures, it is found that the addition of polycarboxylic water reducer can make the distribution of rubber particles more uniform. Within the specification, the dosage of polycarboxylic water reducer is adjusted continuously, and found the optimum dosage is 7.3 kg/m^3. The SCRC with uniform distribution is prepared as shown in Fig. 3. The SCRC beams are shown in Table 3. The SCRC pavement slabs are shown in Table 4.

2.2 The compressive test and the splitting tensile test

Six standard SCRC specimens (size 150×150×150 mm^3) were divided into two groups. The compressive tests and the splitting tensile tests were carried out on standard specimens to determine the relevant parameters of the SCRC, and the tests were carried out on the closed-loop servo-controlled material testing system (MTS 322) of 500-kN capacity. The elastic modulus, Poisson's ratio and compressive strength of SCRC specimens were measured by compression tests. The average values of the three groups of tests were calculated as the material parameters of SCRC (Chen *et al*. 2013). Due to the difficulties of direct tensile testing on concrete, only limited and conflicting data are available (Chen *et al*. 2017). The tensile strength of SCRC specimens was measured by the splitting tensile test. The average value of the three groups was calculated as the tensile strength of SCRC (Qing *et al*. 2018, Chen ***et al***. 2014). According to the test measurement and calculation, the material parameters of the SCRC were determined as shown in Table 5.

Table 4 Condition of the SCRC slab

Experiment type	Fracture type	Specimen size (mm^3)	Number	Loading mode	Loading rate (mm/s)
Slab loading (On soil test)	α=0.3	560×500×100	1	Center test	0.001
	β=0.75	560×500×100	1	Center test	0.001
	α=0.3	560×500×100	1	Eccentric test	0.001
	β=0.75	560×500×100	1	Eccentric test	0.001

Table 5 Material parameters of SCRC

E (GPa)	μ	f_{cu} (MPa)	F_t (MPa)
28.6	0.15	26. 65	1.718

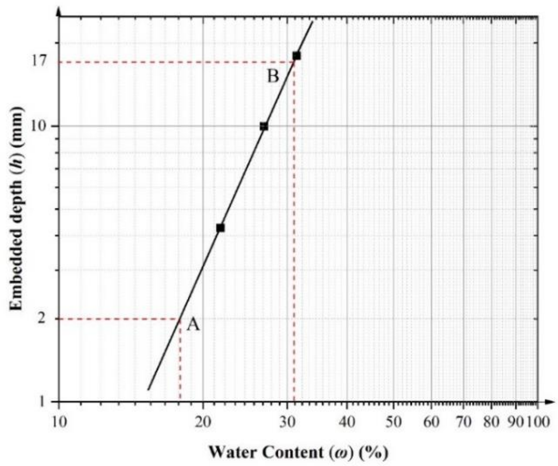

Fig. 4 Relationship between the cone penetration and the water content

Table 6 Liquid-plastic limit data of analysis

ω_L (%)	ω_p (%)	I_p
31	18	13

2.3 Soil material parameters

According to the standard of GB/T 50123-1999, foundation soil samples of three different water content are made. The cone penetration (mm) and water content (%) of each sample were determined using the LP-100 liquid-plastic limit combined instrument. The recorded results are shown in Fig. 4. According to Fig. 4, the plastic limit (A) and the liquid limit (B) can be determined, and the plasticity index can be calculated, as shown in Table 6.

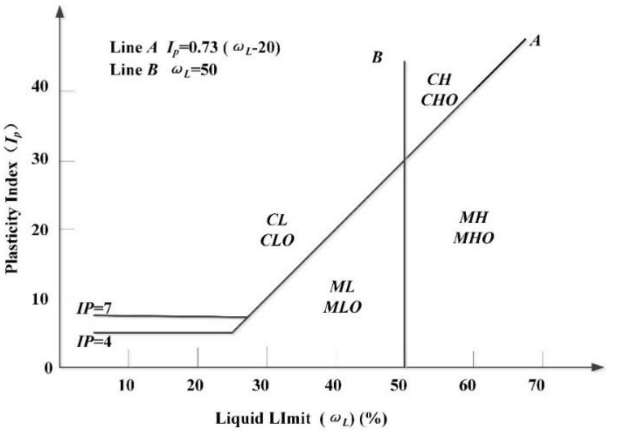

Fig. 5 Relationship between the plastic limit and the liquid limit for 17 mm of water content as liquid limit

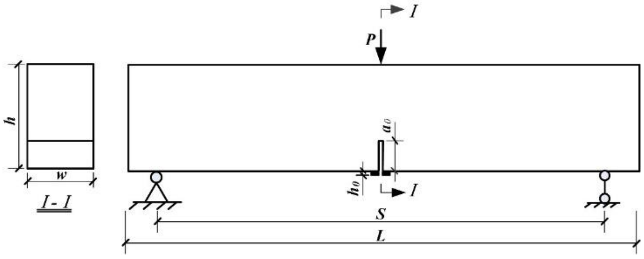

Fig. 6 Loading schematic diagram of SCRC beam on TPB test

(a) 1200×250×100 mm^3

(b) 800×150×100 mm^3

(c) 400×100×100 mm^3

Fig. 7 The TPB test on concrete beams with different dimensions

Fig. 8 SCRC beam on foundation soil test for a schematic diagram

The plasticity index and the liquid limit are determined. In Fig. 5, the CH, CL, MH, ML are high liquid-limit clay, low liquid-limit clay, high liquid-limit silt, low liquid-limit silt respectively. It can be judged from Fig. 5 that the type of foundation soil is the low liquid limit clay.

2.4 SCRC beam on fracture test

2.4.1 SCRC beam on three-point bending (TPB) test

In the TPB test, the displacement-controlled loading was applied to the center SCRC beam by the MTS 322. The force and crack mouth opening displacement (P-CMOD) curve can be measured. The loading mode of the test is the displacement control, and the loading rate is 0.001 mm/s.

The TPB test of the SCRC beam is performed under small deformation, as shown in Fig. 6. The notch/depth ratio is $(a_0+h_0)/(h+h_0)$ and the span is S. The CMOD is measured continuously with the help of a clip gauge. The TPB test has three different sizes, and the crack growth effect of size effect was considered (Guan *et al*. 2016, Trivedi and Singh 2015). Each test was carried out three times. The loading forms were shown in Fig. 7.

2.4.2 SCRC beam on foundation soil test

As the SCRC beams with prefabricated crack performing on foundation soil, it is necessary to improve the loading device. The improved MTS 322 equipment, as shown in Fig. 8.

Ramming the soil to achieve the compactness of foundation soil in practice project. The SCRC beam can be placed on the foundation soil, and the force loaded on the SCRC beam. The loading form is shown in Fig. 9.

3.Test result analysis

3.1 Result analysis of SCRC beam on TPB test

Specimens were loaded by the TPB loading method, until they were damaged. Data of P-CMOD of the whole process was collected, and each dimension of specimens' P-CMOD was measured three times. The typical P-CMOD curves of each size specimen are shown in Fig. 10.

As shown in Fig. 10, the peak load increases gradually with the increase of specimen depth. When the depth is 100

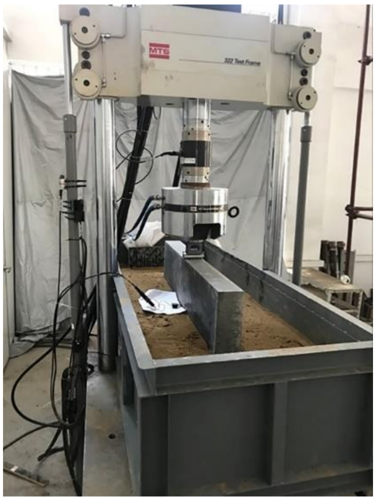

Fig. 9 Foundation bearing test

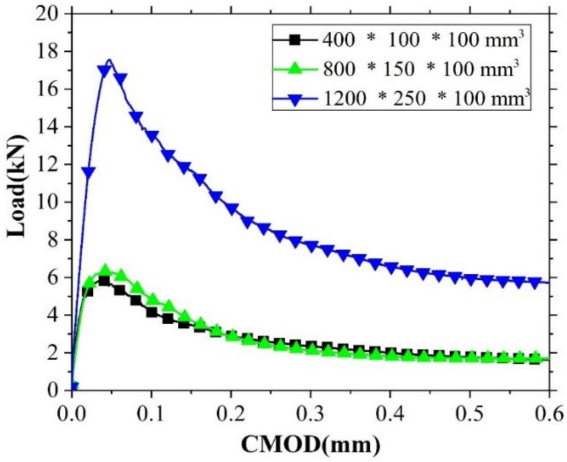

Fig. 11 The P-CMOD curves of SCRC beams on foundation soil test

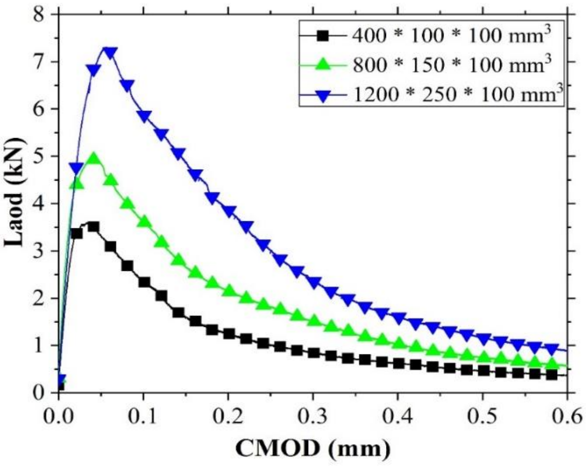

Fig. 10 The P-CMOD curves of SCRC beams on TPB test

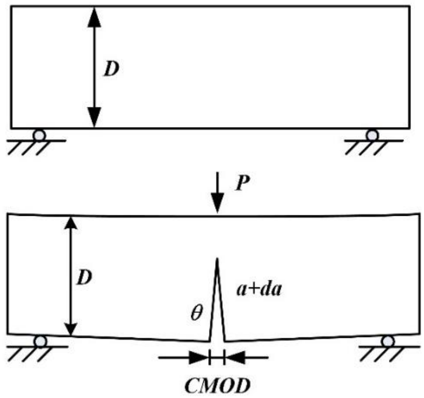

Fig. 12 Deformation schematic diagram of SCRC beam on TPB test

mm, the peak load of the concrete specimen reaches 3.36 kN. When the depth is 250 mm, its peak load increases to 7.30 kN. Guan *et al*. (2016) have proved that the peak load increases with the increase of specimen depth at the same ratio of $(a_0+h_0)/(h+h_0)$for ordinary concrete. Compared with his test results, it was found that the peak load of the SCRC was a little lower than the peak load of ordinary concrete. The ultimate deformation of the SCRC specimens increased significantly with the increase of specimen depth. It can be seen that the size effect on concrete strength is significant. The P-CMOD curve visually proves that the flexural behavior of concrete beam under monotonic loading is affected by the size effect, and the bearing capacity and ductility increase with the increase of specimen depth.

3.2 Result analysis of SCRC beam on foundation soil test

Specimens of this section are the same with Section 3.1. The loading method of specimens with prefabricated cracks the foundation bearing method. The typical P-CMOD curves of specimens of various sizes are shown in Fig. 11.

As shown in Fig. 11, the flexural peak load increases gradually with the increase of specimen depth. When the depth is 100 mm, the peak load of the concrete specimen reaches 5.86 kN. When the depth is 150 mm, the peak load of concrete specimen reaches 6.33 kN, and the bearing capacity increase is not obvious. When the depth is 250 mm, its peak load increases to 17.55 kN, and the bearing capacity increase is obvious. Compared with the results of the TPB test, the bearing capacity of specimens has increased. The P-CMOD curve shows that the bearing capacity of the SCRC beams under monotonic loading is affected by the size and constraint conditions.

3.3 The formulation for fracture parameter

According to the knowledge of fracture mechanics, the fracture energy of the SCRC beam can be calculated by the P-CMOD curves of the TPB test (Hillerborg 1985). The computing method is as follows**:**

The SCRC beam will be deformed with the applied load, as shown in Fig. 12. The beam will rotate along with the tip point of the equivalent virtual crack. By analyzing the Fig. 12, the approximate expression of the rotation angle can be expressed as Eq. (1).

$$\theta = \frac{CMOD}{a + da} \tag{1}$$

The equivalent virtual crack expansion da can be calculated according to Eq. (2) by the P-CMOD curves of the TPB test.

$$da = \frac{2}{\pi} \times \left(h + h_0\right) \times \arctan\left(\sqrt{\frac{E \times t \times CMOD}{32.6 \times P} - 0.1135}\right) - h_0 - a \quad (2)$$

The elastic modulus E in Eq. (2) can be calculated according to Eq. (3).

$$E = \frac{1}{t \times C_i} \times \left[3.70 + 32.60 \times \tan^2\left(\frac{\pi \times a_0 + h_0}{2 \times h + h_0}\right)\right] \quad (3)$$

The initial value C_i (μm/kN) of the specimen in Eq. (3) calculated according to Eq. (4).

$$C_i = \frac{CMOD_i}{P_i} \quad (4)$$

It is assumed that all forces act on the crack propagation, regardless of the dissipation of the external energy in the fracture process zone. According to the definition of work, the work done by the external force can be expressed in Eq. (5).

$$W = \int_0^{\theta_0} \left(M_1 + M_2\right) d\theta \quad (5)$$

The M_1 and M_2 in Eq. (5) are respectively expressed as the bending moment caused by the load (P) and the weight of the SCRC beam, which are calculated by Eq. (6) and Eq. (7).

$$M_1 = \frac{P \times S}{4} \quad (6)$$

$$M_2 = \frac{m \times g \times S}{8} \quad (7)$$

According to the definition of fracture energy in fracture mechanics, the fracture energy can be expressed as Eq. (8) (Zhang and Xu 2008).

$$G_F = \frac{\int P d\theta + 0.5 m g \theta_0}{A} = \frac{\int_0^{\theta_0} P d\theta + 0.5 m g \theta_0}{t \times \left(h - a_0\right)} = \frac{W}{t \times \left(h - a_0\right)} \quad (8)$$

According to the above theory of fracture mechanics, the fracture energy of the various specimens is calculated by P-CMOD curves in MATLAB, as shown in Table 6.

The critical effective crack length is calculated using Eq. (9) as follows

$$a_c = \frac{2}{\pi} \times (h + h_0) \times \arctan\sqrt{\frac{t \times E \times CMOD_C}{32.6 \times P_{\max}} - 0.113} - h_0 \quad (9)$$

The critical stress intensity factor is calculated using the Eq. (10) (Shah 1990).

$$K_{IC}^S = 3 \times (P_{\max} + \frac{0.5mgS}{L}) \times \frac{S \times \sqrt{a_c} \times F(\alpha)}{2 \times t \times h^2} \quad (10)$$

Table 7 Fracture parameter with various specimens

Specimen size (length, depth, width) (mm^3)	a_c (mm)	G_F (N/m)	K_{IC}^S (N/mm$^{3/2}$)
1200×250×100	124.3	127.1	56.5
800×150×100	94.1	121.6	79.9
400×100×100	46.4	119.7	31.0

where $F(\alpha)$ is a function of α, whose expression is as follows:

$$F(\alpha) = \frac{1.99 - \alpha \times (1 - \alpha) \times (2.15 - 3.93 \times \alpha + 2.7\alpha^{2)}}{(1 + 2\alpha) \times (1 - \alpha)^{1.5}} \quad (11)$$

where α is as follows

$$\alpha = \frac{(a_c + h_0)}{(h + h_0)} \quad (12)$$

The critical stress intensity factor K_{IC}^S is calculated as shown in Table 7. Ulfkjaer *et al*. (1996) had studied the fracture energy of ordinary concrete. Compared with his test results, the fracture energy of SCRC was relatively large, which indicated that the addition of rubber particles could improve the ductility of concrete.

4. Numerical simulation

4.1 Extended finite element theory

In 1999, Beleytachko of the Northwestern University of America proposed the XFEM (Belytschko *et al*. 2009, Ooi and Yang 2010, Guiamatsia *et al*. 2009). The method is an important improvement to the traditional finite element method. The core idea of the XFEM is to represent the discontinuity in the computational region by extending the shape function with discontinuous property. In the process of calculation, the description of discontinuous field is entirely independent of the mesh boundary. By using the XFEM, the crack propagation path can be simulated conveniently, and the heterogeneous materials with holes and inclusions can be simulated.

In the XFEM, the mesh and crack are independent of each other, so the local mesh encryption method is unnecessary for crack propagation. The crack surface doesn't need to be the element edge and the crack tip doesn't need to be the element node. It can simplify pretreatment and improve calculative efficiency. The mesh density has a remarkable effect on the stress intensity factors, as shown in Fig. 13. By using XFEM, fracture simulation of SCRC beam can be convenient. Using reasonable mesh density can also get a reliable result.

4.2 Numerical simulation of TPB

In this paper, a mathematical model of crack propagation is established utilizing the linear softening method in Abaqus. The dimension of the XFEM model are the same as the specimens in practice. The dimensions of

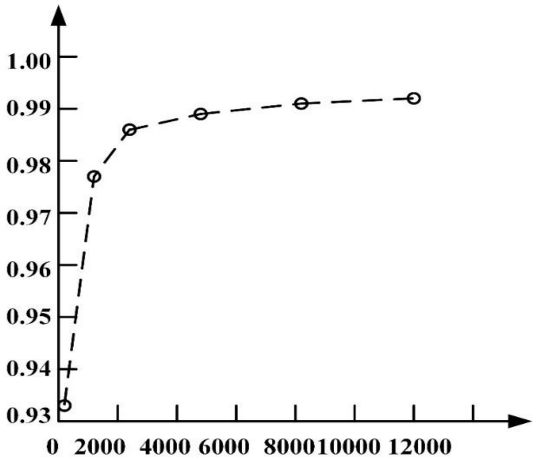

Fig. 13 Effect of mesh density on stress intensity factor

Table 8 Material properties of XFEM model for TPB

Model name	1200×250×100 (mm^3)	800×150×100 (mm^3)	400×100×100 (mm^3)
E (GPa)	28.6	28.6	28.6
μ	0.15	0.15	0.15
f_{cu} (MPa)	26.65	26.65	26.65
f_t (MPa)	1.718	1.718	1.718
G_F (N/m)	127.1	121.6	119.1
Density (kg/m^3)	2100	2100	2100
Damage criterion	MAXPS	MAXPS	MAXPS

the specimens are 1200×250×100 mm^3, 800×150×100 mm^3 and 400×100×100 mm^3 respectively. The initial crack-depth ratio (α) is 0.3 and the span-depth ratio is 0.75. The displacement load applies to the center of span. Parameters of the SCRC are shown in Table 8. The type of softening stage is set to linear. Although the failure process of concrete is nonlinear, the linear softening model can generally meet the calculation requirements (Xu and Needleman 1994, Ioannides and Peng 2004). Professor Hillerborg assumes that the type of softening stage is linear when simulating the damage of concrete. The linear softening model can predict the flexural capacity of the experimental slabs reasonably (Sallier and Forquin 2012).

The mesh generation of the model is based on the eight-node hexahedron element. The XFEM model does not need to take local mesh encryption at the crack tip. The simulations are calculated with different mesh sizes, finding that when the mesh size is smaller than a value, the simulation results have nothing to do with mesh size, the mesh size can be determined.

By comparing the P-CMOD curves of numerical simulation and test, the type of damage evolution, the softening stage type, the damage evolution coefficient and the mesh size are determined. The type of damage evolution is energy. The type of softening stage is linear. The mixed mode behavior of the softening stage is power law. The softening stage coefficient is 0.09. Considering the influence of different mesh sizes, the model with different mesh sizes is established (Zhou and Lu 2018). The sides of

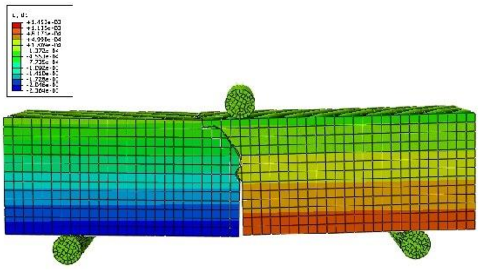

(a) 400×100×100 mm^3

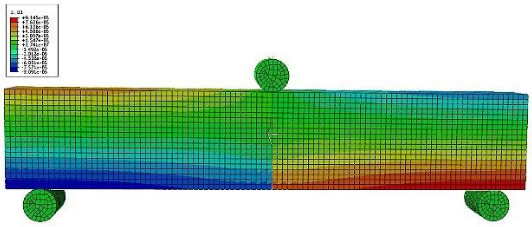

(b) 800×100×150 mm^3

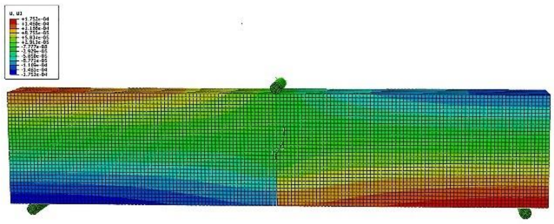

(c) 1200×100×250 mm^3

Fig. 14 Total displacement cloud picture of TPB model

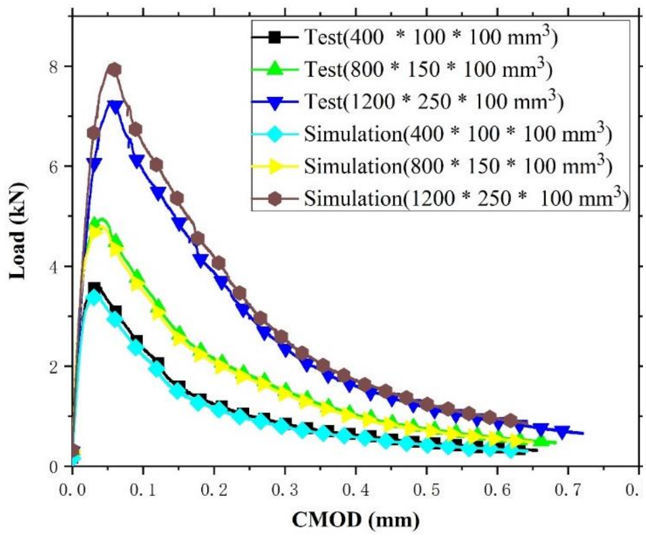

Fig. 15 Comparison of numerical simulation and test results of beams on TPB

the mesh are 0.008 m. The viscosity coefficient of damage stability is 0.002. The setting of the TPB model can be determined.

Analyzing the cloud picture total displacement under the TPB model, as shown in Fig. 14, the total displacement of the model is symmetrical, which conforms to the force condition. The cloud picture shows that the crack tip keeps expanding until beam damages. It reflects the actual process of crack propagation.

Table 9 Material parameter of XFEM model for foundation bearing

Material types	Model name	1200×250×100 (mm^3)	800×150×100 (mm^3)	400×100×100 (mm^3)
Self-compacting rubberized concrete (SCRC)	E (GPa)	28.6	28.6	28.6
	μ	0.15	0.15	0.15
	f_{cu} (MPa)	26.65	26.65	26.65
	f_t (MPa)	1.718	1.718	1.718
	G_F (N/m)	127.1	121.6	119.1
	Density (kg/m^3)	2100	2100	2100
	Softening stage coefficient	0.09	0.09	0.09
	viscosity coefficient	0.002	0.002	0.002
Damage criterion		MAXPS	MAXPS	MAXPS
Foundation soil	E (GPa)	80	80	80
	μ	0.25	0.25	0.25
	Density (kg/m^3)	1700	1700	1700
	o_u (Pa)	4100	4100	4100
	Friction angle (°)	18.1	18.1	18.1
	Dilatancy angle (°)	14	14	14

Comparing the P-CMOD curves of numerical simulation and test, as shown in Fig. 15, they are consistent, proving that the softening stage coefficient and the mesh size are appropriate.

4.3 Numerical simulation of the foundation bearing

In Section 4.2, the parameters of the SCRC are determined. In this section, the contact between the SCRC and the foundation soil needs to be determined. In Section 2.3, the liquid-plastic limit combined measurement is adopted, finding that the foundation soil is cohesive soil. According to soil mechanics, the Mohr-Coulomb yielding criteria is applicable to calculate the yielding of cohesive soil. The friction angle and cohesion of the cohesive soil should be determined. In general, determining friction angle and cohesion of the soil needs to conduct a field test. This paper did not conduct the field test, but has adopted the range of the relevant parameters of cohesive soil from relevant specification. By comparing the P-CMOD curves of numerical simulation with the test date, the boundary condition of the SCRC can be determined. The normal direction is the hard touching, the tangential direction is the frictional effect, and the penalty is 0.15. The set value of related material parameters is shown in Table 9.

As for the foundation soil, according to the accuracy and the time of the calculation, the eight-node hexahedron element is adopted, and the sides of mesh are 0.04 m.

Analyzing the total displacement cloud picture of the foundation bearing model, as shown in Fig. 16, the total displacement of the model is symmetrical, which conforms to the force condition of the SCRC beam. The size of the foundation model is 2000×700×400 mm^3 (long, wide, high), which is much bigger than the concrete beam. Only part of the foundation soil model is shown in the cloud pictures.

Comparing the P-CMOD curves of the numerical simulation and test, as shown in Fig. 17, they are consistent, so the boundary conditions of the SCRC beams are determined.

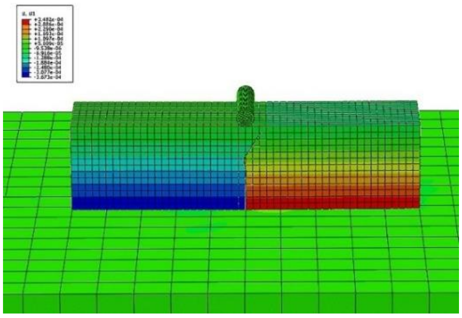

(a) 400×100×100 mm^3

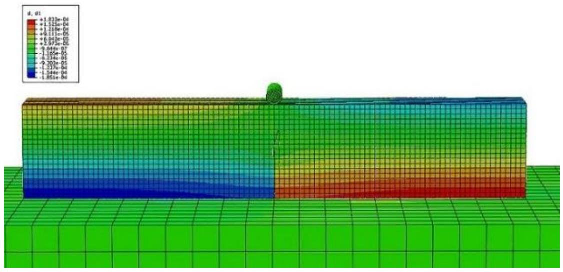

(b) 800×150×100 mm^3

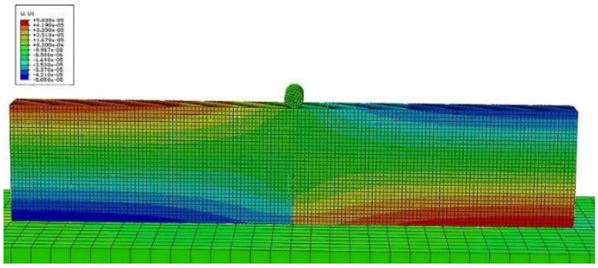

(c) 1200×250×100 mm^3

Fig. 16 Total displacement cloud picture of foundation bearing model

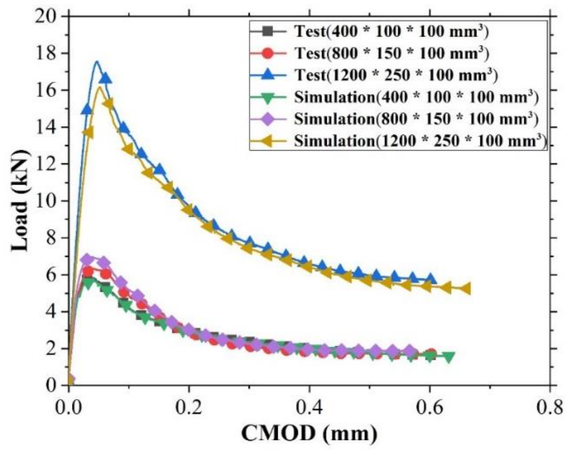

Fig. 17 Comparison of numerical simulation and test results of beams on foundation soil

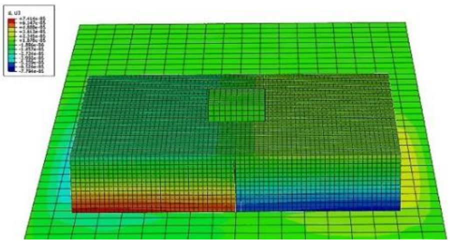

(a) Center test and α=0.3

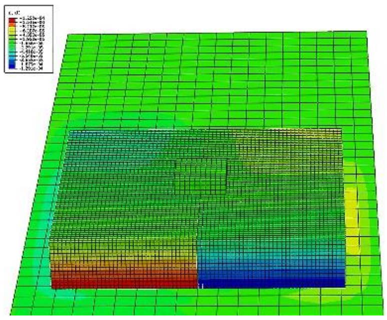

(b) Center test and β=0.75

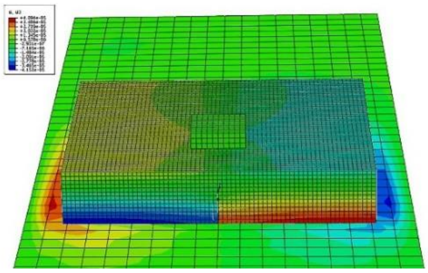

(c) Eccentric test and α=0.3

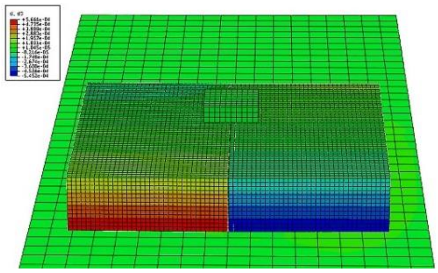

(d) Eccentric test and β=0.75

Fig. 18 Total displacement cloud picture of a predictive model

Fig. 19 Loading form of foundation bearing displacement loading control method

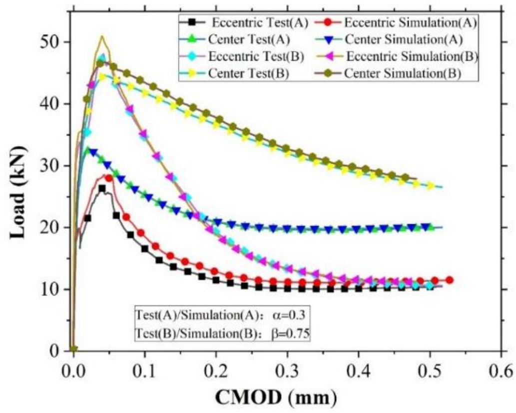

Fig. 20 Comparison of numerical simulation and test results of slabs on foundation soil

4.4 The construction of the predictive model

Based on the above analysis, the softening stage coefficient, mesh size and boundary condition of the SCRC can be determined, and the prediction model of the SCRC pavement slab can be constructed under these conditions. The fracture process of the SCRC pavement slabs can be predicted. There are many types of cracks and loading conditions in the actual project. Using Abaqus, the prediction models of different types of cracks and loading positions are constructed, and the total displacement cloud pictures of the models are shown in Fig. 18.

5. Validation of the predictive model and discussions

To verify the reliability of the predictive model, the model is validated by the corresponding test with the predictive model. The loading form of the SCRC pavement slab is shown in Fig. 19.

Comparing the P-CMOD curves of numerical simulation and test, as shown in Fig. 20, they are consistent. Hence, the predictive model is reliable. As can be seen from the Fig. 20, the peak load of the longitudinal penetrating crack is much larger than that of the transverse penetrating crack. Therefore, in a practical project, effective prevention measures should be taken for the transverse penetrating cracks. The failure stage of central loading test is much gentler than that of the eccentric loading test, which indicates that the specimen under eccentric loading is more likely to fail after reaching a peak load.

6. Conclusions

This paper investigates the fracture properties of the SCRC pavement slab. An XFEM model for predicting the fracture process of SCRC pavement slabs is constructed. The main conclusions are as follows:

• Compared with ordinary concrete, the uniaxial compressive strength, tensile strength and flexural strength of the SCRC are lower. However, the strength of SCRC still meets the requirement of pavement. On the premise of satisfying the strength, the SCRC can increase the ductility of pavement slab.

•·The results of the SCRC beams test show that the bearing capacity of SCRC beams decreases with the increasing of the specimen depth at the same initial crack-depth ratio. The P-CMOD curve proves visually that the bearing capacity increase with the increase of specimen depth. The results of the SCRC slab test and numerical simulation show that the bearing capacity of concrete slab is affected by the type of crack and the loading location. With the same type of crack, the bearing capacity of concrete slab of the eccentric loading test is higher than that of central loading test. With the same loading location, the bearing capacity of the lateral penetrating crack is higher than that of the underside penetrating crack.

• A predictive model for the fracture process of SCRC is essential for mechanistic design of SCRC used in applications with traffic loading. After obtaining the parameters for the SCRC based on the small-scale beams test results, the predictive models were generated to predict the fracture properties of the SCRC pavement slabs. The predictive model applies to types of cracks and various loading positions.

Acknowledgements

The research is based upon the work supported by the Open Foundation of State Key Laboratory of Hydrology-Water Resources and Hydraulic Engineering (2017491711).

References

Belytschko, T., Gracie, R. and Ventura, G. (2009), “TOPICAL REVIEW: A review of extended/generalized finite element methods for material modeling”, *Model. Simul. Mater. SC.*, **17**(4).

Bu, J.W., Chen, X.D., Liu, S.S., Li, S.T. and Shen, N. (2018), “Experimental study on the dynamic behavior of pervious concrete for permeable pavement”, *Comput. Concrete*, **22**(3), 291-303. https://doi.org/10.12989/cac.2018.22.3.291.

Chen, X., Bu, J., Fan, X., Lu, J. and Xu, L. (2017), “Effect of loading frequency and stress level on low cycle fatigue behavior of ordinary concrete in direct tension”, *Constr. Build. Mater.*, **133**, 367-375. https://doi.org/10.1016/j.conbuildmat.2016.12.085.

Chen, X., Wu, S. and Zhou, J. (2013), “Experimental study and analytical formulation of mechanical behavior of concrete”, *Constr. Build. Mater.*, **47**(10), 662-670. https://doi.org/10.1016/j.conbuildmat.2013.05.041.

Chen, X., Wu, S. and Zhou, J. (2014), “Strength values of cementitious materials in bending and tension test methods”, *J. Mater. Civil Eng.*, **26**(3), 484-490. https://doi.org/10.1061/(ASCE)MT.1943-5533.0000846.

Dong, W., Zhang, X., Zhang, B. and Wu, Q. (2018), “Influence of sustained loading on fracture properties of concrete”, *Eng. Fract. Mech.*, **200**, 134-145. https://doi.org/10.1016/j.engfracmech.2018.07.034.

Fakhri, M. and Amoosoltani, E. (2017), “Crack behavior analysis of roller compacted concrete mixtures containing reclaimed asphalt pavement and crumb rubber”, *Eng. Fract. Mech.*, **180**, 43-59. https://doi.org/10.1016/j.engfracmech.2017.05.011.

Gaedicke, C., Roesler, J. and Evangelista Jr, F. (2012), “Three-dimensional cohesive crack model prediction of the flexural capacity of concrete slabs on soil”, *Eng. Fract. Mech.*, **94**, 1-12. https://doi.org/10.1016/j.engfracmech.2012.04.029.

Gao, H. (2007), “Influence factors analysis of broken slab on cement concrete pavement”, *Forest Eng.*, 4.

Gencel, O., Ozel, C., Brostow, W. and MartÃ-nez-Barrera, G. (2015), “Mechanical properties of self-compacting concrete reinforced with polypropylene fibres”, *Mater. Res. Innov.*, **15**(3), 216-225. https://doi.org/10.1179/143307511X13018917925900.

Guan, J., Hu, X. and Li, Q. (2016), “In-depth analysis of notched 3-p-b concrete fracture”, *Eng. Fract. Mech.*, **165**, 57-71. https://doi.org/10.1016/j.engfracmech.2016.08.020.

Guiamatsia, I., Falzon, B.G., Davies, G.A.O. and Iannucci, L. (2009), “Element-free Galerkin modelling of composite damage”, *Compos. Sci. Technol.*, **69**(15-16), 2640-2648. https://doi.org/10.1016/j.compscitech.2009.08.005.

Hesami, S., Hikouei, I.S. and Emadi, S.A.A. (2016), “Mechanical behavior of self-compacting concrete pavements incorporating recycled tire rubber crumb and reinforced with polypropylene fiber”, *J. Clean. Prod.*, **133**, 228-234. ps://doi.org/10.1016/j.jclepro.2016.04.079.

Hillerborg, A. (1985), “The theoretical basis of a method to determine the fracture energy GF of concrete”, *Mater. Struct.*, **18**(4), 291-296. https://doi.org/10.1007/BF02472919.

Hou, Y., Yue, P., Xin, Q., Pauli, T. and Sun, W. (2014), “Fracture failure of asphalt binder in mixed mode (Modes I and II) by using phase-field model”, *Road Mater. Pavement*, **15**(1), 167-181. https://doi.org/10.1080/14680629.2013.866155.

Ioannides, A.M. and Peng, J. (2004), “Finite element simulation of crack growth in concrete slabs: Implications for pavement design”, *Proceedings of the Fifth International Workshop on Fundamental Modeling of Concrete Pavements*, Istanbul, Turkey, April.

Khaloo, A.R., Dehestani, M. and Rahmatabadi, P. (2008), “Mechanical properties of concrete containing a high volume of tire-rubber particles”, *Waste Manage.*, **28**(12), 2472-2482. https://doi.org/10.1016/j.wasman.2008.01.015.

Kim, H.B. and Lee, S.H. (2002), “Reliability-based design model applied to mechanistic empirical pavement design”, *KSCE J. Civil Eng.*, **6**(3), 263-272. https://doi.org/10.1007/BF02829149.

Kumar, S., Singh, I.V. and Mishra, B.K. (2014), “XFEM simulation of stable crack growth using J-R, curve under finite strain plasticity”, *Int. J. Meth. Mater. Des.*, **10**(2), 165-177. https://doi.org/10.1007/s10999-014-9238-1.

Long, G., Gao, Y. and Xie, Y. (2015), “Designing more sustainable and greener self-compacting concrete”, *Constr. Build. Mater.*, **84**, 301-306. https://doi.org/10.1016/j.conbuildmat.2015.02.072.

Merhej, T. and Feng, D.C. (2011), “Parameter sensitivity analysis of airport rigid pavement thickness using FAARFIELD program”, *Adv. Mater.*, **243-249**, 4068-4074. https://doi.org/10.4028/www.scientific.net/AMR.243-249.4068.

Modarres, A. and Shabani, H. (2015), “Investigating the effect of aircraft impact loading on the longitudinal top-down crack propagation parameters in asphalt runway pavement using fracture mechanics”, *Eng. Fract. Mech.*, **150**, 28-46. https://doi.org/10.1016/j.engfracmech.2015.10.024.

Najim, K.B. (2012), “Mechanical and dynamic properties of self-compacting crumb rubber modified concrete”, *Constr. Build. Mater.*, **27**(1), 521-530.

https://doi.org/10.1016/j.conbuildmat.2011.07.013.

Ooi, E.T. and Yang, Z.J. (2010), "A hybrid finite element-scaled boundary finite element method for crack propagation modelling", *Comput. Method. Appl. M.*, **199**(17-20), 1178-1192. https://doi.org/10.1016/j.cma.2009.12.005.

Qing, L., Shi, X., Mu, R. and Cheng, Y. (2018), "Determining tensile strength of concrete based on experimental loads in fracture test", *Eng. Fract. Mech.*, **202**, 87-102. https://doi.org/10.1016/j.engfracmech.2018.09.017.

Sallier, L. and Forquin, P. (2012), "On the use of Hillerborg regularization method to model the softening behaviour of concrete subjected to dynamic tensile loading", *E. EPJ-Spec. Topic.*, **206**(1), 97-105. https://doi.org/10.1140/epjst/e2012-01591-5.

Shah, S.P. (1990), "Determination of fracture parameters (K_{ICS} and $CTOD_C$) of ordinary concrete using three-point bend tests", *Mater. Struct.*, **23**(6), 457-460. https://doi.org/10.1007/BF02472029.

Singh, I.V., Mishra, B.K., Bhattacharya, S. and Patil, R.U. (2012), "The numerical simulation of fatigue crack growth using extended finite element method", *Int. J. Fatig.*, **36**(1), 109-119. https://doi.org/10.1016/j.ijfatigue.2011.08.010.

Skarżyński, Ł., Nitka, M. and Tejchman, J. (2015), "Modelling of concrete fracture at aggregate level using FEM and DEM based on X-ray μCT images of internal structure", *Eng. Fract. Mech.*, **147**, 13-35. https://doi.org/10.1016/j.engfracmech.2015.08.010.

Sukontasukkul, P. and Chaikaew, C. (2006), "Properties of concrete pedestrian block mixed with crumb rubber", *Constr. Build. Mater.*, **20**(7), 450-457. https://doi.org/10.1016/j.conbuildmat.2005.01.040.

Reda Taha, M.M., El-Dieb, A.S., Abd El-Wahab, M.A. and Abdel-Hameed, M.E. (2008), "Mechanical, fracture, and microstructural investigations of rubber concrete", *J. Mater. Civil Eng.*, **20**(10), 640-649. https://doi.org/10.1061/(ASCE)0899-1561(2008)20:10(640).

Tao, M. (2017), "Application of waste rubber asphalt mixture in the pavement maintenance", *Transport. Sci.*.

Trivedi, N. and Singh, R.K. (2015), "Chattopadhyay, Investigation on fracture parameters of concrete through optical crack profile and size effect studies", *Eng. Fract. Mech.*, **147**, 119-139. https://doi.org/10.1016/j.engfracmech.2015.08.027.

Turgut, P. and Yesilata, B. (2008), "Physico-mechanical and thermal performances of newly developed rubber-added bricks", *Energy Build.*, **40**(5), 679-688. https://doi.org/10.1016/j.enbuild.2007.05.002.

Ulfkjaer, J.P., Hansen, L.P., Qvist, S. and Madsen, S.H. (1996), "Fracture energy of ordinary concrete beams at different rates of loading", *Struct. Shock Impact IV.*, **25**, 1-11. https://doi.org/10.2495/SUSI960381.

Venkateswara, R.S., Seshagiri, R.M.V. and Ramaseshu, D. Rathish, K.P. (2012), "Durability performance of self-compacting concrete", *Biomed. Chromatogr.*, **16**(1), 31-40. https://doi.org/10.1016/j.conbuildmat.2012.07.049.

Wang, H.Y. (2012), "Reason analysis and processing method of cement concrete pavement broken slab", *Shanxi Architecture*. **2012**(33), 92.

Xu, X.P. and Needleman, A. (1994), "Numerical simulations of fast crack growth in brittle solids", *J. Mech. Phys. Solid.*, **42**(9), 1397-1434. https://doi.org/10.1016/0022-5096(94)90003-5.

Yung, W.H., Yung, L.C. and Hua, L.H. (2013), "A study of the durability properties of waste tire rubber applied to self-compacting concrete", *Constr. Build. Mater.*, **41**(41), 665-672. https://doi.org/10.1016/j.conbuildmat.2012.11.019.

Zak, A., Krawczuk, M. and Ostachowicz, W. (2006), "Propagation of in-plane waves in an isotropic panel with a crack", *Finite Elem. Anal. Des.*, **42**(11), 929-941. https://doi.org/10.1016/j.finel.2006.01.013.

Zhai, C., Wang, X., Kong, J., Li, S. and Xie, L. (2017), "A sophisticated simulation for the fracture behavior of concrete material using XFEM", *Earthq. Eng. Eng. Vib.*, **16**(4), 859-881. https://doi.org/10.1007/s11803-017-0393-x.

Zhang, X.F. and Xu, S.l. (2008), "Determination of fracture energy of three-point bending concrete beam using relationship between load and crack-mouth opening displacement", *J. Hydraul. Eng.*, **39**(6), 714-719.

Zheng, L., Huo, X.S. and Yuan, Y. (2008), "Strength, modulus of elasticity, and brittleness index of rubberized concrete", *J. Mater. Civil. Eng.*, **20**(11), 692-699. https://doi.org/10.1061/(ASCE)0899-1561(2008)20:11(692).

Zhou, R. and Lu, Y. (2018), "A mesoscale interface approach to modelling fractures in concrete for material investigation", *Constr. Build. Mater.*, **165**, 608-620. https://doi.org/10.1016/j.conbuildmat.2018.01.040.

Zhu, X.Y., Chen, X.D., Shen, N., Tian, H.X., Fan, X.Q. and Lu, J. (2018), "Mechanical properties of pervious concrete with recycled aggregate", *Comput. Concrete.*, **21**(6), 623-635. https://doi.org/10.12989/cac.2018.21.6.623.

Zi, G. and Belytschko, T. (2010), "New crack-tip elements for XFEM and applications to cohesive cracks", *Int. J. Numer. Meth. Eng.*, **57**(15), 2221-2240. ttps://doi.org/10.1002/nme.849.

HK

Nomenclature

a	crack length (m)
a_0	initial crack length (m)
da	crack growth increment (m)
E	elastic modulus (GPa)
f_{cu}	compressive strength (MPa)
F_t	tensile strength (MPa)
g	acceleration of gravity (9.18 m/s^2)
G_F	fracture energy (N/m)
h	depth of beam (m)
h_0	the thickness of the edge steel sheet of the clip gauge (m)
I_P	plasticity index
L	length of beam (m)
m	mass between the bearing of specimen (kg)
w	width of beam (m)
ω_L	liquid limit
ω_P	plastic limit
S	span of beam (m)
α	initial crack-depth ratio
β	initial crack- width ratios
θ	rotation angle of beam (°)
σ_u	yield stress